Flying Qubit Investigations for Heterostructure-based Qubit Implementations

Haozhi Dong
Department of Electrical and Computer Engineering
Michigan State University
East Lansing, MI, USA
donghao2@msu.edu

Gaurab Panda
Department of Electrical and Computer Engineering
Michigan State University
East Lansing, MI, USA
pandagau@msu.edu

Kan Xie
Department of Electrical and Computer Engineering
Michigan State University
East Lansing, MI, USA
xiekan@msu.edu

Virginia Ayres
Department of Electrical and Computer Engineering
Michigan State University
East Lansing, MI, USA
ayresv@msu.edu

Harry Shaw
Code 5660
NASA Goddard Space Flight Center
Greenbelt, MD, USA
harry.c.shaw@nasa.gov

Deborah Preston
Advanced Special Studies
Univeristy of Maryland
College Park, MD, USA
dmpreston@terpmail.umd.edu

Manohar Deshpande
Code 5550
NASA Goddard Space Flight Center
Greenbelt, MD, USA
manohar.d.deshpande@nasa.gov

***Abstract*—Flying qubit designs have emerged as a new approach for adding dynamic control to solid-state qubit implementations including heterostructure-based electron gas implementations. The flying qubit approach utilizes the potential minimum of a SAW wave for the capture and transport of a single or few electron(s) from a reduced dimensionality electron pool. Many details of the interactions between the dynamic potential well induced by propagating SAW wave with the reduced dimensionality electron pool are unknown. In the present work, we investigate the effect of the SAW wave longitudinal component modelled as perturbation to the k-space momentum in the transport direction for a heterostructure-based finite width 1D channel. A new quadratic expression for the k-space momentum and a new expression for the number density are reported for the first time. A major effect of positive or negative longitudinal perturbations on electron transport is the introduction of shifts that can affect both quantum channel accessibility and number density allowed occupations.**

Keywords— Quantum Information Processing; Modeling and Simulation of Nanostructures and Nanodevices; Nanoelectronics

I. Introduction

Quantum communications refer to communication systems that are based on quantum entanglement. These systems may be realized using laser-based and solid-state implementations. Solid-state implementations are preferred whenever space, mass and/or thermal restrictions are key to operations, while laser-based implementations are preferred for high-speed, long distance operations. The present research focuses on a solid-state qubit implementation achieved using a heterostructure-based reduced dimensionality electron gas to generate a pool of electrons whose properties can be manipulated to produce exact one-state and then entangled two-state systems based on electron spin. The basic configuration, of a 2D heterostructure implemented in a GaAs-AlGaAs stack with a 1D channel created using split-gate technology, was previously reported [1] and shown to be a viable basis for spin-based qubit implementations. The focus of the present investigation is on the means to exert an additional layer of dynamic control over both confinement and coherent transport through use of the "flying qubit" design.

By themselves, the electrons in the 1D channel are insufficiently uniform, even with external magnetic control, to produce a pool of single spin state electrons. They also undergo too many scattering events for transport to be coherent over a typical channel length. Flying qubit designs have emerged as a new approach for adding dynamic control to solid-state qubit implementations including heterostructure-based electron gas implementations [1]. The flying qubit approach utilizes the potential minimum of a surface acoustic wave (SAW) for the capture and transport of a single or few electron(s) from a reduced dimensionality electron pool. The concept was inspired by experimentally demonstrated single electron capture and transport by SAW waves, including capture from reduced dimensionality 0D quantum dots, with transport over several microns of distance [2].

A flying qubit design for an ideal heterostructure-based 1D channel was explored in Ref. [1] and found to be viable; however, many details of the interactions between the dynamic potential induced by propagating SAW wave with the reduced dimensionality electron pool were not investigated. One key aspect not previously reported is that a SAW wave consists of a longitudinal as well as a

National Aeronautics and Space Administration Grant NNX16AT85G.

transverse component. In the present work, we focus on the effects of the longitudinal component interaction with the reduced dimensionality 1D electron pool and find that it can significantly influence both transport uniformity and transmission. Furthermore, the present analysis is developed for a realistic finite width 1D channel.

II. RESULTS AND DISCUSSION

A. Finite Width Channel

Key features of the configuration are identified in Fig. 1. GaAs-AlGaAs layers are used to create a 2D quantum well in the z-direction (dotted line) and a split gate introduces additional confinement in the y-direction that depends on width W (inset above). The actual motion of the GaAs substrate in response to the propagating SAW wave is a retrograde motion that includes both longitudinal and transverse components (inset above).

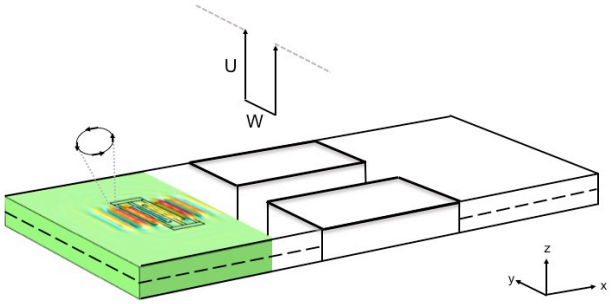

Fig. 1. 2D quantum well in z dotted line) with additional width W dependent quantum well in y (inset above). GaAs response to propagating SAW wave includes both longitudinal and transverse components (inset above).

We first formulate 1D number density n_L (#/length) for electrons in the channel and then investigate how this is impacted by the addition of the SAW wave potential longitudinal component. When the z- and y-confinements are modeled using an infinite potential well approximation, 3D unrestricted motion (equation (1)) is reduced to 1D in the x-direction (equation (2)). E_C is the GaAs bandgap energy, 1.43 eV.

$$E = E_C + \frac{\hbar^2 k_x^2}{2m_x^*} + \frac{\hbar^2 k_y^2}{2m_y^*} + \frac{\hbar^2 k_z^2}{2m_z^*} \tag{1}$$

$$E = E_C + \frac{\hbar^2 k_x^2}{2m_x^*} + \frac{n_y^2 \pi^2 \hbar^2}{2m_y^* L_y^2} + \frac{n_z^2 \pi^2 \hbar^2}{2m_z^* L_z^2} \tag{2}$$

If the lowest energy level 2D quantum well and the bandgap energy are combined in E_S and the width W dependent 1D quantum well is investigated at its lowest energy level E_1, then:

$$E_S = E_C + \frac{1^2 \pi^2 \hbar^2}{2m_z^* L_z^2} \tag{3}$$

$$E_1 = 1^2 \left(\frac{\pi^2 \hbar^2}{2m_y^* W^2} \right) \tag{4}$$

$$E = E_S + \frac{\hbar^2 k_x^2}{2m_x^*} + i^2 E_1 \tag{5}$$

$$k_{x,i} = \sqrt{\frac{2m_x^*}{\hbar^2}(E - E_S - i^2 E_1)} \tag{6}$$

The number density n_L in the channel is investigated in the degenerate regime as the energy level limitations in the reduced dimensionality material force the fermi energy level E_f above the bottom of the conduction band:

$$n_L = \int N(E) O(E_f - E) dE \tag{7}$$

The total number density of states in k-space, when converted to E-space using equation (6), gives:

$$N_T(\bar{k}) = N_T(k_{x,i}) = \frac{2k_{x,i} x 2}{(n_x = 1)\frac{2\pi}{L_x}}$$

$$\Rightarrow N_T(E) = L_x \frac{2}{\pi} \sum_i \sqrt{\frac{2m_x^*}{\hbar^2}(E - E_S - i^2 E_1)} \tag{8}$$

which produces an energy density of states N(E) and a number density n_L given by:

$$N(E) = \frac{2}{\pi} \frac{d}{dE} \left(\sum_i \sqrt{\frac{2m_x^*}{\hbar^2}(E - E_S - i^2 E_1)} \right) \tag{9}$$

$$n_L = \int \frac{2}{\pi} \frac{d}{dE} \left(\sum_i \sqrt{\frac{2m_x^*}{\hbar^2}(E - E_S - i^2 E_1)} \right) O(E_f - E) dE \tag{10}$$

$$n_L = \frac{2}{\pi} \sum_i \sqrt{\frac{2m_x^*}{\hbar^2}(E - E_S - i^2 E_1)} \tag{11}$$

Conventionally, dimensionless $n_L W$ is investigated through multiplication by $1 = E_1/E_1$ while using the effective mass near equality $m_x^* = m_y^* = m_z^*$ in GaAs as a direct bandgap material.

$$n_L W = 2\sum_{i=1}\sqrt{\frac{(E_f - E_S)}{E_1} - i^2} \qquad (12)$$

and plotted with $x = (E_f - E_S)/E_1$ as a running variable as shown in Fig. (2). Specific values can be identified by matching the 2D-1D boundary conditions:

$$E_f - E_S = \frac{n_S}{\frac{m^*}{\pi\hbar^2}} \qquad (13)$$

The dotted lines in Figure 2 show GaAs results for $n_S = 5 \times 10^{11}$ cm^{-2} with $m^* = 0.07\ m_0$. The E_1 values (equation (4)) correspond to widths W = 1000 Angstroms (Å), 500 Å and 100 Å. For 1000 Å and 500 Å, there are, respectively, 5 and 3 channels available for transport. For 100 Å, there is no transport because E_f-E_S/E_1 is below the cut-off for the i = 1 channel.

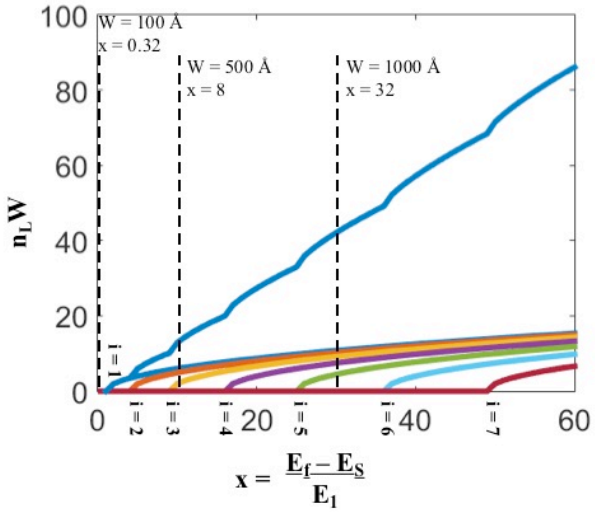

Fig. 2. Normalized 1D electron number density. The number of channels available for transport has dropped from 5 to 3 to none as a function of the channel width.

B. Longitudinal Perturbation

If n_L is not normalized as dimensionless as in equation (12), then the number density is given by:

$$n_L = \frac{2}{\pi}\sum_i \sqrt{\frac{\pi^2}{W^2}\left(\frac{(E_f - E_S)}{E_1} - i^2\right)} \qquad (14)$$

The width-dependent number densities for W = 1000 Å and 500 Å are shown in Figure (3a) and 3(d). As expected, n_L is higher in the narrower channel. Another effect of the finite width W seen in both Figure 3(a) and (d) and also in Figure (2) is the rounded nature of each step, in contrast to a textbook 1D flat-step staircase [3].

The effect of the SAW wave longitudinal component is to introduce a perturbation to the local potential that can impact the x-momentum:

$$p_x \Longrightarrow p_x + dp_x \qquad (15)$$

$$\hbar k_x \Longrightarrow \hbar(k_x + \epsilon) \qquad (16)$$

When the derivation of n_L is repeated with this perturbation included, a new quadratic expression for k_x is found in which equation (21) replaces equation (6):

$$\frac{\hbar^2 k_x^2}{2m^*} \Longrightarrow \frac{\hbar^2}{2m^*}(k_x^2 + 2\epsilon k_x + \epsilon^2) \approx \frac{\hbar^2}{2m^*}(k_x^2 + 2\epsilon k_x) \qquad (17)$$

$$E = E_S + \frac{\hbar^2}{2m^*}(k_x^2 + 2\epsilon k_x) + i^2 E_1 \qquad (18)$$

$$k_{x,i}^2 + 2\epsilon k_{x,i} = \frac{2m^*}{\hbar^2}(E - E_S - i^2 E_1) = C(i) \qquad (19)$$

$$k_{x,i}^2 + 2\epsilon k_{x,i} - C(i) = 0 \qquad (20)$$

$$k_{x,i} = \frac{-2\epsilon \pm \sqrt{(2\epsilon)^2 - 4(1)(-C(i))}}{2(1)} = -\epsilon \pm \sqrt{\epsilon^2 + C(i)} \qquad (21)$$

This produces an energy density of states N(E) and a number density n_L given by:

$$N(E) = \frac{1}{L_x}\frac{d}{dE}\left(L_x \frac{2}{\pi}\sum_i\left(-\epsilon \pm \sqrt{\epsilon^2 + C(i)}\right)\right) \qquad (22)$$

$$n_L = \frac{2}{\pi}\sum_i\left(-\epsilon \pm \sqrt{\epsilon^2 + \left[\frac{\pi^2}{W^2}\left(\frac{E_f - E_S}{E_1} - i^2\right)\right]}\right) \qquad (23)$$

Equation (23) reduces to equation (14) when ϵ goes to zero.

C. Effects on Uniformity and Transport

The effects of perturbation ϵ on transport in the $+k_x$ direction are considered in this paper:

$$n_L = \frac{2}{\pi}\sum_i\left(-\epsilon + \sqrt{\epsilon^2 + \left[\frac{\pi^2}{W^2}\left(\frac{E_f - E_S}{E_1} - i^2\right)\right]}\right) \qquad (24)$$

Because the second term under the square root is scaled by π^2/W^2, the numerical value of ϵ can be large yet remain small in comparison. Values of $\epsilon = \pm 10^8$ were used to investigate this effect. Both positively and negatively signed perturbations $\pm\epsilon$ are shown to

influence n_L, through the introduction of shifts that affect both quantum channel accessibility and number density n_L allowed occupation. The results for physical channel width W = 1000Å are shown in Figure 3. The quantum "staircase" is shifted toward lower values on the normalized energy x-axis by an amount equal to 10.1 for both $\pm\epsilon$.

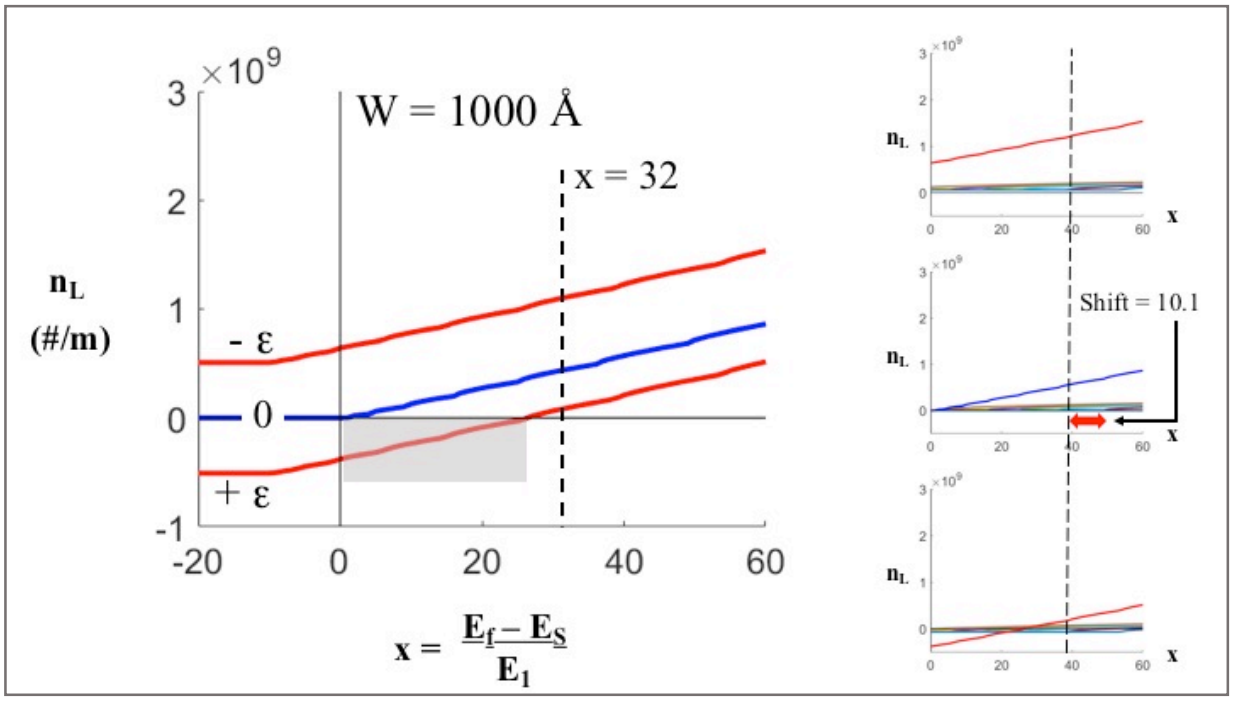

Fig. 3. For width W = 1000Å, longitudinal perturbations shift the quantum "staircase" up or down by approximately by $\pm\epsilon$ and towards lower normalized energy values by an amount 10.1, reducing the quantum channel accessibility and changing the number density n_L allowed occupation.

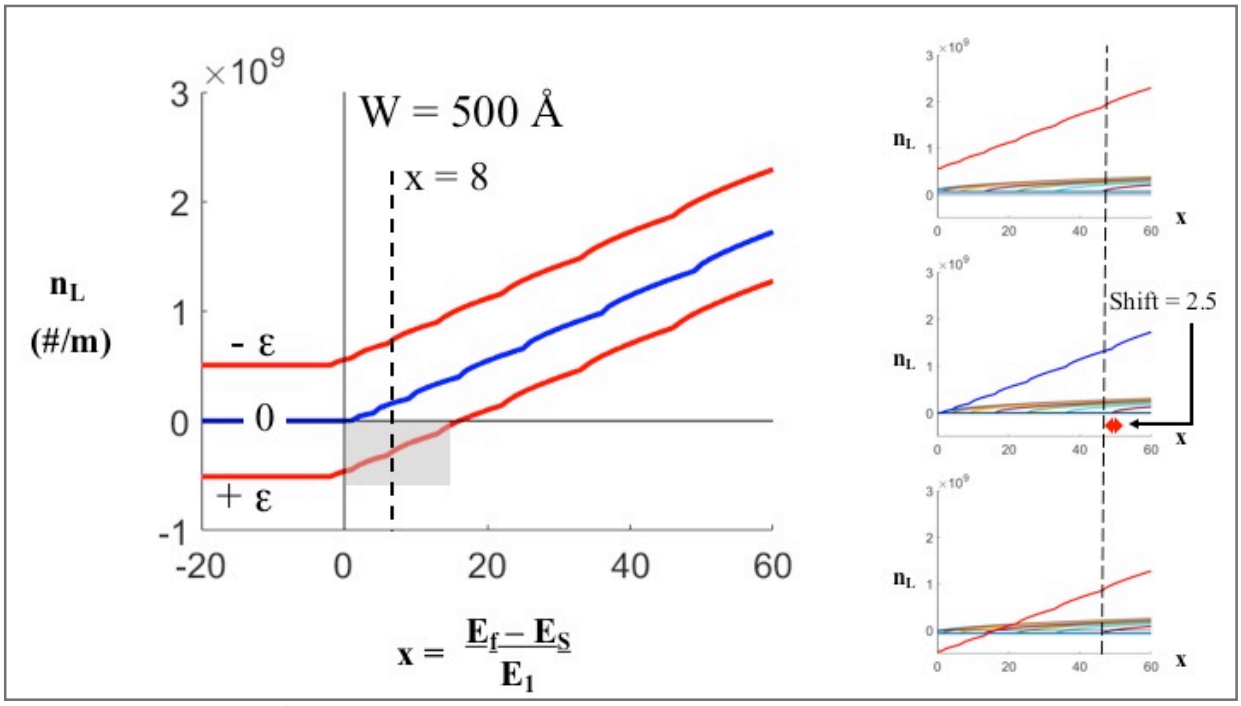

Fig. 4. For width W = 500Å, longitudinal perturbations shift the quantum "staircase" up or down by approximately by ±ϵ and towards lower normalized energy values by an amount 2.5, reducing the quantum channel accessibility, to 0 for the +ϵ longitudinal perturbation, and changing the number density n_L allowed occupation.

Further shifts dominated by $\pm\epsilon$ appear on the number density n_L y-axis. For the previously investigated normalized energy of $(E_f - E_S)/E_1 = 32$, the $-\epsilon$ longitudinal perturbation reduces the number of quantum channels (staircase "steps") available for transport from 5 to 3, although a higher n_L occupancy is allowed. For the $+\epsilon$ longitudinal perturbation part of the retrograde motion cycle, the number of quantum channels available for transport is reduced from 5 to 1, with a lower allowed n_L occupancy.

The results for physical channel width W = 500Å are shown in Figure 4. The quantum "staircase" is shifted toward lower values on the normalized energy x-axis by an amount equal to 2.5 for both $\pm\epsilon$, and up and down on the number density n_L y-axis by approximately $\pm\epsilon$. For the previously investigated normalized energy of $(E_f - E_S)/E_1 = 8$, the $-\epsilon$ longitudinal perturbation reduces the number of quantum channels available for transport from 3 to 1, with a higher n_L occupancy. From a uniformity perspective, this may be a desirable outcome. For the $+\epsilon$ longitudinal perturbation part of the retrograde motion cycle, there are 0 quantum channels available for transport.

III. CONCLUSIONS

Flying qubit designs have emerged as a new approach for adding dynamic control to solid-state qubit implementations including heterostructure-based electron gas implementations. The flying qubit approach utilizes the potential minimum of a SAW wave for the capture and transport of a single or few electron(s) from a reduced dimensionality electron pool. Many precise details of the interactions of the dynamic potential induced by propagating SAW wave with the reduced dimensionality electron pool remain to be investigated. In the present work, we have investigated the SAW wave longitudinal component modelled as perturbation to the local potential that can impact the k_x momentum in the transport direction. This led to the derivation of a new quadratic expression for k_x (equation (21)) and a new expression for n_L (equation (24)).

A major effect of positive or negative longitudinal perturbations on $+k_x$ electron transport is the introduction of shifts that can affect both quantum channel accessibility and number density n_L allowed occupations. This indicates that the longitudinal component of SAW wave retrograde surface motion needs to be taken into account in heterostructure-based flying qubit designs. Furthermore, the reduction in quantum channel accessibility indicated by our results could, with careful device engineering, lead to implementations with a more uniform electron pool, which can be more easily aligned into uniform spin states for entanglement. Work is continuing in our group to explore increasingly accurate SAW wave-electron pool interaction models to guide experimental tests.

ACKNOWLEDGMENT

The support of National Aeronautics and Space Administration Grant NNX16AT85G is gratefully acknowledged.

REFERENCES

[1] C. H. W. Barnes, J. M. Shilton, A. M. Robinson, "Quantum Computation Using Electrons Trapped by Surface Acoustic Waves", Physical Review B, vol. 62, pp. 8410-8419, 2000.

[2] R. P. G. McNeil1, M. Kataoka, C. J. B. Ford, C. H. W. Barnes, D. Anderson, G. A. C. Jones, I. Farrer, D. A. Ritchie, "On-demand Single-electron Transfer Between Distant Quantum Dots", Nature, vol. 477, pp. 439-442, 2010.

[3] S. Datta, Electronic Transport in Mesoscopic Systems. Cambridge, UK, Cambridge University Press, 1997, chs. 1-2.